Near-infrared organic photodetectors based on bay-annulated indigo showing broadband absorption and high detectivities up to 1.1 mu m

Peer-reviewed author version

VERSTRAETEN, Frederik; GIELEN, Sam; VERSTAPPEN, Pieter; KESTERS, Jurgen; Georgitzikis, Epimitheas; RAYMAKERS, Jorne; Cheyns, David; Malinowski, Pawel; DAENEN, Michael; LUTSEN, Laurence; VANDEWAL, Koen & MAES, Wouter (2018) Near-infrared organic photodetectors based on bay-annulated indigo showing broadband absorption and high detectivities up to 1.1 mu m. In: JOURNAL OF MATERIALS CHEMISTRY C, 6 (43), p. 11645-11650.

DOI: 10.1039/c8tc04164d
Handle: http://hdl.handle.net/1942/27909

Near-infrared organic photodetectors based on bay-annulated indigo showing broadband absorption and high detectivities up to 1.1 µm

Frederik Verstraeten[a,†], Sam Gielen[a,†], Pieter Verstappen[a], Jurgen Kesters[a], Epimitheas Georgitzikis[b,c], Jorne Raymakers[a], David Cheyns[b], Pawel Malinowski[b], Michaël Daenen[a,d], Laurence Lutsen[a,d], Koen Vandewal[a,d], Wouter Maes[a,d,*]

[a] UHasselt – Hasselt University, Institute for Materials Research (IMO), Agoralaan 1 – Building D, 3590 Diepenbeek, Belgium

[b] IMEC, Kapeldreef 75, 3001 Leuven, Belgium

[c] ESAT, Katholieke Universiteit Leuven, Kasteelpark Arenberg 10, 3001 Leuven, Belgium

[d] IMEC, Associated Lab IMOMEC, Wetenschapspark 1, 3590 Diepenbeek, Belgium

[†] These authors contributed equally.

Abstract

Near-infrared photodetection is valuable for numerous scientific, industrial and recreational applications. The implementation of organic semiconductors in near-infrared photodetectors offers additional advantages, such as printability on flexible substrates, reduced manufacturing costs and facile tuning of the detection range. In this work, the nature-inspired bay-annulated indigo (BAI) dye is employed as a building block for near-infrared sensitive, push-pull type conjugated polymers. The electron-deficient BAI moiety is copolymerized with a set of electron-rich monomers, affording polymers with an absorption onset up to 1300 nm and a sufficiently high lowest unoccupied molecular orbital, allowing electron transfer to standard fullerene acceptors. Bulk heterojunction type organic photodetectors are fabricated and the resulting device characteristics are analysed. The best performing photodetector is based on the polymer **PTTBAI** comprising thieno[3,2-*b*]thiophene as the electron-rich moiety. It has a superior light to dark current ratio, with a dark current density of 10^{-7} A/cm², resulting in a (shot-noise limited) detectivity of 10^{12} Jones at -2 V bias within the spectral window of 600−1100 nm, exceeding the detectivity of conventional silicon CCD photodetectors in the near-infrared region (~10^{11} Jones).

Introduction

The field of organic electronics has afforded emerging technologies such as organic light-emitting diodes (OLEDs),[1] photovoltaics (OPVs)[2] and photodetectors (OPDs)[3]. For the latter, enhanced detectivities, extended absorption windows, smaller pixel sizes and lower manufacturing costs are targeted towards scientific, industrial and communal applications.[4–6] More specifically, the detection of wavelengths in the near-infrared (NIR) region (800-3000 nm)[7] is appealing for applications ranging from industrial inspection and sorting, to safety, security and life sciences.[8–10]

Nowadays, near-infrared photodetectors (NIR-PDs) are commonly based on inorganic semiconductors such as InGaAs or HgCdTe. The devices are fabricated in a hybrid configuration, requiring the use of micro bumps as electrical interconnections to the CMOS (complementary metal oxide semiconductor) readout circuit, resulting in increased manufacturing costs and limited pixel sizes.[11–16] NIR organic photodetectors could overcome these problems as they can be manufactured monolithically, resolving the interconnection issues. As a result, the pixel size and active area can be reduced, thus increasing the resolution and lowering the costs. Additionally, organic semiconductors can be deposited by printing technologies onto various light-weight and flexible substrates, allowing large area processing.[17,18] Moreover, they allow fine-tuning of the optoelectronic characteristics through dedicated material design.

Only a handful of reasonably well performing NIR-OPDs are reported in the literature, in general aiming at high detectivities over a broad wavelength range spanning the visible and part of the NIR region. Heeger *et al.* for example reported a high-detectivity photodetector with a spectral response from 300 to 1450 nm based on a NIR-sensitive copolymer combining thieno[3,4-*c*][1,2,5]thiadiazole as the electron-poor and 2,2':5',2''-terthiophene as the electron-rich monomer.[4] Their OPDs gave detectivities exceeding 10^{12} Jones at 800 nm and a linear dynamic range over 100 dB. More recently, Azoulay and co-workers obtained detectivities exceeding 10^{11} Jones within the spectral range of 600–1430 nm, together with a measurable detectivity up to 1800 nm, by employing PCPDTBT (poly[2,6-(4,4-dialkyl-4*H*-cyclopenta[2,1-*b*;3,4-*b'*]dithiophene)-*alt*-4,7-(2,1,3-benzothiadiazole)] and its bridgehead imine-substituted analogue as NIR-sensitive copolymers.[19] Wang *et al.* developed a NIR-absorbing copolymer based on the electron-rich, disc-like dithienobenzotrithiophene (DTBTT) and the electron-poor thienoisoindigo (TII) building block.[20] The resulting OPD device showed a detectivity in the order of 10^{12} Jones within the range of 300–1000 nm, exceeding 10^{10} Jones up to 1600 nm.

From an application point of view, photodetection at wavelengths around 940 nm is particularly attractive. As 940 nm illumination sources are readily available, integration in multiple applications can be foreseen, such as basic wildlife cameras, automotive tools (*e.g.* monitoring the surroundings of a car) and virtual/augmented reality (*e.g*. eye tracking and gesture recognition).[8–10] Since the detectivity (D^*), the most important figure of merit for photodetectors, is dictated by the external quantum efficiency (EQE) alongside with the dark current density (J_D), the employed photoactive polymers have to be specifically designed to absorb strongly in this region of the NIR. To achieve this goal, the 'strong donor – strong acceptor' approach can be used.[21] This implies copolymerization of very electron-rich and very electron-deficient heteroaromatic monomers in an alternating fashion, resulting in polymers with strong intramolecular charge transfer characteristics, shifting the absorption maximum to the NIR part of the spectrum. It has already been shown that the absorption onset of conjugated polymers can be extended to wavelengths over 2000 nm using this strategy.[22]

In this study, a relatively new electron-poor monomer based on bay-annulated indigo (BAI) is employed for the preparation of polymer semiconductors with an absorption maximum around 940 nm. BAI-based materials were introduced a few years ago in OPV devices[23–27] and have promising

characteristics for NIR-OPDs as well. The strong electron-withdrawing properties and relatively high lowest unoccupied molecular orbital (LUMO) energy levels render the BAI core a perfect candidate for NIR-sensitive push-pull type electron donor copolymers. Furthermore, as a result of the large planar structure, the tendency for π-π stacking is rather high, which is beneficial for intermolecular charge transport.[23,24,28] Additionally, the synthesis of BAI requires the low-cost natural dye indigo as a precursor, from which several thousands of tons are produced every year.[29] In this work, a strongly electron-deficient novel BAI-based monomer is copolymerized with a set of heterocyclic monomers of varying electron-donating strength. The influence of the polymer structure on its optoelectronic properties is investigated and the BAI-based polymers are shown to be suitable candidates for 940 nm photodetection, with absorption onset wavelengths down to 1300 nm. The polymers are then incorporated in photodetector devices and the NIR-OPD characteristics are compared. The best performing NIR-OPD is based on a polymer combining BAI and thieno[3,2-*b*]thiophene and achieves a specific detectivity of approximately 10^{12} Jones, a linear dynamic range of 145 dB and rise and fall times of 25 and 30 µs, respectively. As such, this photodetector can compete with conventional silicon CCD detectors in the 940 nm region.[30]

Results and discussion

The formation of the BAI core, *via* the bay-annulation of indigo, results in a large planar and rigid structure and concomitant solubility and purification problems.[27,31] Therefore, an optimized synthetic pathway towards a more soluble, thiophene flanked BAI-based monomer was developed (Scheme 1). The long and branched 2-octyldodecyl side chain on the thiophene moieties ensures solubility without (too much) hampering the π-π stacking of different BAI cores. First, 4-bromothiophene-2-acetic acid was protected and alkylated by the iodine functionalized alkyl chain **1** *via* a cobalt catalyzed reductive alkylation as reported by Liu *et al.*[32] The ester group of product **3** was then saponified and converted to an acid chloride. The subsequent bay annulation of the natural dye indigo afforded BAI derivative **5** in a relatively low yield. Nonetheless, optimization by changing the solvent from toluene to xylene, together with a higher reaction temperature and lower addition rate of the acid chloride solution, did increase the yield from 14 to 31%. Finally, dibromination with *N*-bromosuccinimide afforded the required BAI monomer **6**, which is, despite the rigid core, highly soluble in chloroform.

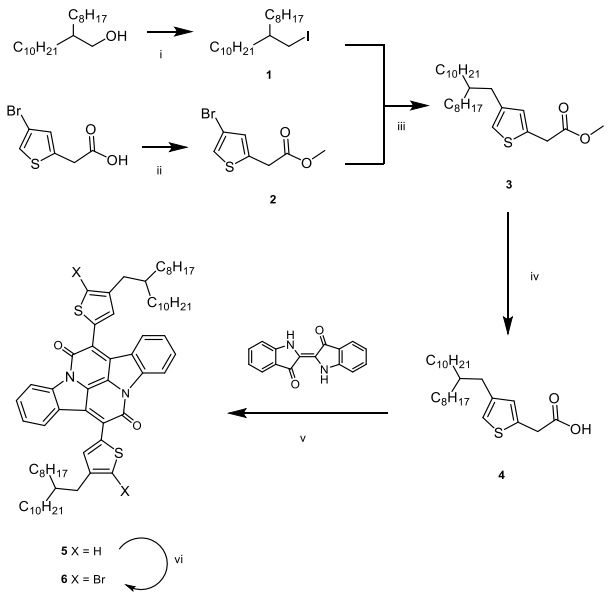

Scheme 1. *Synthetic pathway towards the BAI monomer: i) imidazole, PPh_3, I_2, THF, RT (83%); ii) $SOCl_2$, MeOH, RT (98%); iii) $CoBr_2$, P(p-tolyl)$_3$, Mn powder, TFA, DMAc-pyridine, 50 °C (52%); iv) $LiOH.H_2O$, THF-water, reflux (95%); v) $SOCl_2$, xylene, reflux (31%); vi) NBS, chloroform, RT (72%).*

The BAI monomer was then copolymerized with six different distannylated electron-rich monomers through Stille polycondensation (Figure 1). These monomers were based on known building blocks from the OPV field, such as cyclopenta[2,1-*b*:3,4-*b*']dithiophene (CPDT; **PCPDTBAI**), thiophene (T; **PTBAI**), thieno[3,2-*b*]thiophene (TT; **PTTBAI**) and dithieno[3,2-*b*:2',3'-*d*]pyrrole (DTP; **PDTPBAI**).[33] To further decrease the bandgap, the ladder-type building block thieno[2',3':4,5]thieno[3,2-*b*]thieno[2',3':4,5]thieno[2,3-*d*]pyrrole (TTP; **PTTPBAI**) was employed as an additional electron-donating monomer.[34] The final monomer was based on 2,2'-(2,5-difluoro-1,4-phenylene)dithiophene (DFB; **PDFBBAI**), inspired by the recent work by Lee *et al.*, in which the dark current of OPD devices was drastically decreased by copolymerizing with this difluorobenzene-based donor.[35]

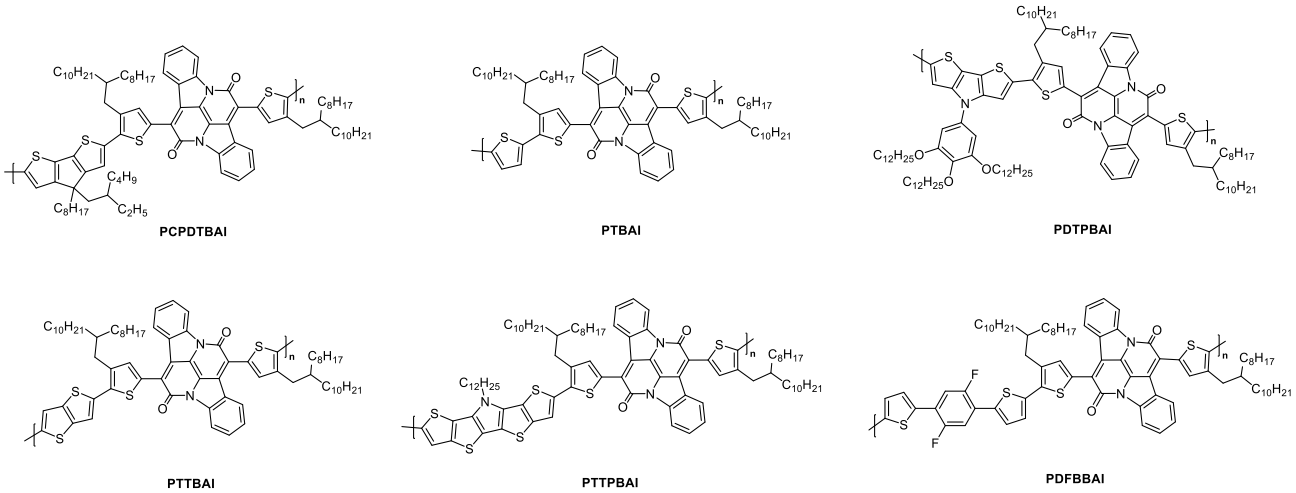

Figure 1. *Chemical structures of the synthesized BAI-based polymers.*

The resulting copolymers were purified by successive Soxhlet extractions. Notably, a very low solubility was observed for **PTTPBAI** and **PDFBBAI** (<1 mg/mL in chlorobenzene). The molar mass for the former could not be determined by size exclusion chromatography (SEC), whereas very low numbers were obtained for the latter, possibly due to precipitation of the initial oligomers formed. This limited solubility inhibited further processing of these materials. For **PTBAI**, **PTTBAI**, **PDTPBAI** and **PCPDTBAI**,

the obtained molar masses were adequate for device fabrication. A summary of the polymer characteristics is given in Table 1 and the VIS-NIR absorption spectra are provided in Figure 2.

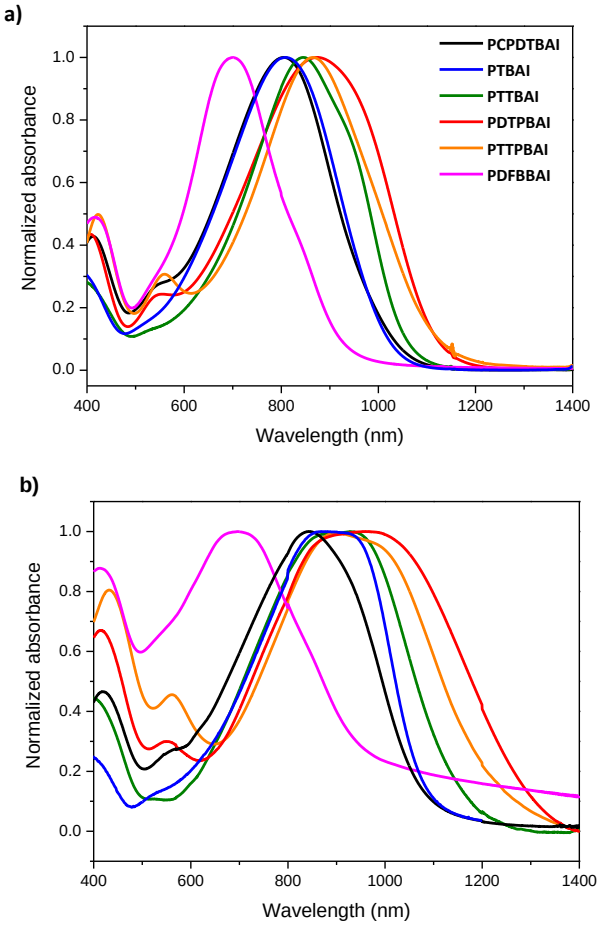

Figure 2. *VIS-NIR absorption spectra of the BAI-based polymers in a) solution, and b) drop-casted film.*

Table 1. *Molar mass, optical and electrochemical properties of the BAI-based copolymers.*

Polymer	M_n[a] (kg/mol)	$Đ$	$\lambda_{max\ film}$[b] (nm)	E_{red}[c] (V)	E_{ox}[c] (V)	E_{LUMO}[d] (eV)	E_{HOMO}[d] (eV)	$E_{g\ opt}$[e] (eV)	$E_{g\ cv}$[f] (eV)
PCPDTBAI	10.8	2.1	844	−1.12	0.34	−3.78	−5.24	1.15	1.46
PTBAI	19.4	2.0	911	−1.17	0.35	−3.80	−5.31	1.14	1.51
PTTBAI	40.5	1.8	929	−1.11	0.29	−3.79	−5.19	1.10	1.40
PDTPBAI	25.1	1.8	963	−1.11	0.19	−3.79	−5.09	0.94	1.30
PTTPBAI	N.A.	N.A.	898	−1.14	0.08	−3.84	−5.06	1.07	1.22
PDFBBAI	4.6	1.3	715	−1.16	0.38	−3.75	−5.29	1.31	1.55

[a] Measured by SEC at 140 °C in *o*-dichlorobenzene.
[b] Films were prepared by drop-casting a solution of the polymer onto a quartz disc.
[c] Onset potentials vs Fc/Fc^+.
[d] Determined from the onset of oxidation/reduction in CV.
[e] Optical bandgap, determined by the onset of the solid-state VIS-NIR spectrum.
[f] Electrochemical bandgap.

Cyclic voltammetry (CV) measurements were performed to estimate the frontier orbital energy levels of the polymer series. As expected, a consistent LUMO value in the range of −3.8 eV was observed for all polymers, since the LUMO level is mainly determined by the electron-poor BAI building block. On the other hand, a variation in the highest occupied molecular orbital (HOMO) energy levels was seen.

More precisely, the HOMO level increased with the electron-donating strength of the comonomer, with a concomitant decrease in (electrochemical) bandgap. This trend is also reflected in the VIS-NIR absorption spectra of the corresponding polymers, which show a red-shift upon increasing electron-donating strength (Figure 2). From these spectra, it is also clear that all polymers, with the exception of **PDFBBAI** (which consists of the less electron-rich fluorinated phenyl building block), have a strong absorption in the targeted 940 nm region.

The influence of the electron-donating building block on the OPD device characteristics was then investigated through the fabrication of bulk heterojunction organic photodetectors in an ITO/PEIE/donor:$PC_{71}BM$/MoO_3/Ag inverted device architecture. The current density-voltage (*J-V*) characteristics under dark (J_D) and illuminated (J_{ph}) conditions (Figure 3a), the external quantum efficiency (EQE, Figure 3b) and the specific detectivity (*D**) (Figure 3c) for all optimized devices are shown in Figure 3. OPD fabrication details and optimization tables can be found in the ESI.

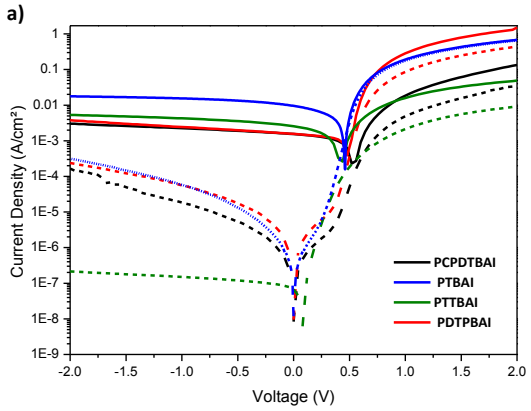

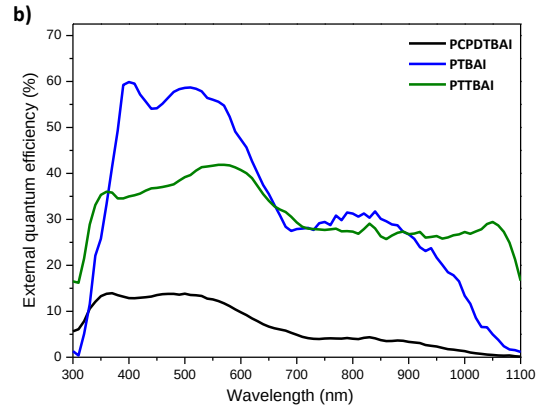

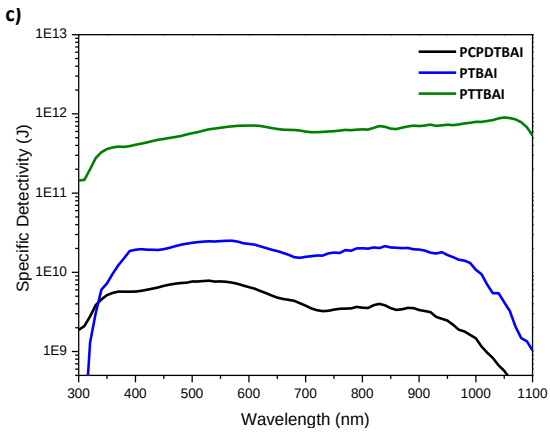

Figure 3. *a) J-V curves measured in darkness (dashed lines) and under illumination (full lines) for optimized NIR-OPD devices based on the BAI polymer series, b) EQE spectra at -2 V, and c) calculated specific detectivities.*

The *J-V* curves in Figure 3a illustrate that the devices based on **PTBAI** and **PTTBAI** perform better with respect to J_{ph} and J_D. Although the J_{ph} is not a figure of merit for OPDs, it is correlated to the EQE, as shown in Figure 3b. **PTBAI** gives the highest EQE (peak near 60% in the VIS) at a reverse bias of −2 V. However, **PTTBAI** performs better in the NIR region, with an EQE around 30% up to 1100 nm. Furthermore, the dark current density at −2 V for the OPD made from **PTBAI** is rather high ($3x10^{-4}$ A/cm²) as compared to the much lower value ($2x10^{-7}$ A/cm²) for **PTTBAI**. In comparison, **PCPDTBAI** and **PDTPBAI** both afford a higher J_D and lower J_{ph}, and consequently a lower EQE. For **PDTPBAI**, noise dominated the EQE spectrum, resulting in a low light current to noise current ratio and yielding unreliable values at negative bias.

The specific detectivity *D** is dominated by both the dark current density and the EQE. Under the assumption of shot-noise only, *D** is given by the following equation:

$$D^* = \frac{\Re}{\sqrt{2qJ_D}} \qquad (1)$$

with $\mathcal{R}$ the responsivity, q the elementary charge of an electron and J_D the dark current density at a specific voltage (here −2 V). Equation (1) neglects thermal and flicker noise. The *D** calculated via equation (1) is therefore an upper-limit of the true specific detectivity.[36] The responsivity $\mathcal{R}$ can be calculated from the EQE spectrum using:

$$\Re = EQE\,\frac{q\lambda}{hc} \qquad (2)$$

As a consequence of equations (1) and (2), a high EQE in combination with a low J_D is favourable. As enhanced read-out speeds are preferred towards applications, EQEs and J_Ds at −2 V bias were employed. The highest detectivity was achieved for the OPDs based on **PTTBAI**, yielding a value of approximately 10^{12} Jones for the spectral region from 600 up to 1100 nm (Figure 3b). The detectivity for the OPD device made from **PTBAI** was lower, despite the higher EQE, because of the higher J_D, yielding a value of approximately 10^{10} Jones in the 400–1000 nm region. The lower J_D for the device based on **PTTBAI** compared to **PTBAI** can be attributed to the thicker active layer of the former (270 vs 130 nm). The effect of decreasing dark current upon increasing active layer thickness is common in organic photodetectors and is also visualized in Figure S3.[37] **PCPDTBAI** showed an even lower *D** ($5x10^9$ Jones) as a consequence of the lower EQE.

To get a better understanding on the variation in performance of the different photoactive materials, the active layer blends were investigated with atomic force microscopy (AFM). Figure 4 shows the topography of the different blends after device optimization. From these images, it can clearly be seen that the **PCPDTBAI** and **PDTPBAI** blends have a completely different topology, indicating phase separation, potentially increasing the J_D and decreasing the EQE as a poorly mixed donor:acceptor blend is unfavourable for photocurrent generation. On the other hand, the active layers based on **PTBAI** and **PTTBAI** showed a nicely intermixed morphology, assisting to the higher EQEs and lower J_D.

In addition, space charge limited current (SCLC) measurements were performed to compare the hole mobilities of the different active layers. As mobilities were all in the order of 10^{-4} cm²/Vs, no specific conclusions could be drawn from these measurements.

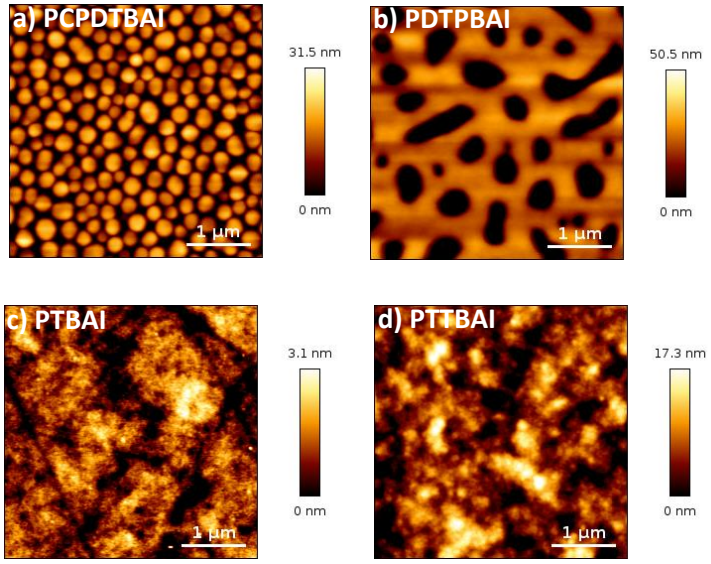

Figure 4. *AFM images of NIR-OPD devices based on a)* ***PCPDTBAI****, b)* ***PDTPBAI****, c)* ***PTBAI*** *and d)* ***PTTBAI****.*

Finally, the rise (t_r) and fall (t_f) time together with the linear dynamic range (LDR) were determined for the NIR-OPD based on **PTTBAI** to get a complete view of the photodetector performance. The t_r and t_f were calculated from the measurement depicted in Figure 5a. LED light (λ = 940 nm, rise (fall) time of 1 (0.5) µs) pulsed with a frequency of 3000 Hz illuminated the **PTTBAI** device. The time needed to get the photocurrent signal from 10 to 90% (t_r) corresponds to 25 µs, and from 90 to 10% (t_f) to 30 µs. From Figure 5b, it can be seen that the LDR covers over 7 orders of magnitude, corresponding to a magnification of 145 dB ($20\text{Log}(I_{max}/I_{min})$). This value is among the highest reported so far for polymer based photodetectors and is larger than the values for Si (120 dB) and InGaAs photodetectors (66 dB),[4] illustrating the capacity of NIR-OPDs to outperform their inorganic analogues. Higher LDR values have been obtained for IR blind perovskite based photodetectors, reaching a measure-limited LDR of approximately 170 dB.[38]

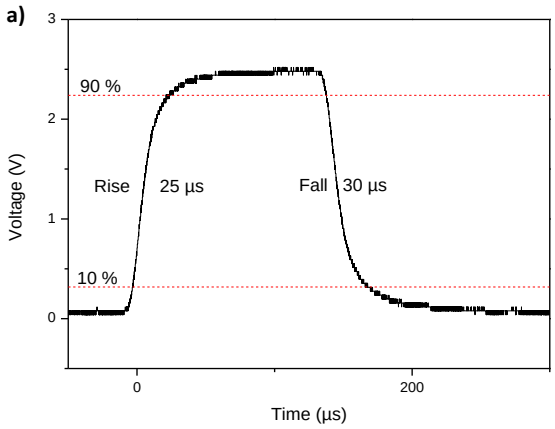

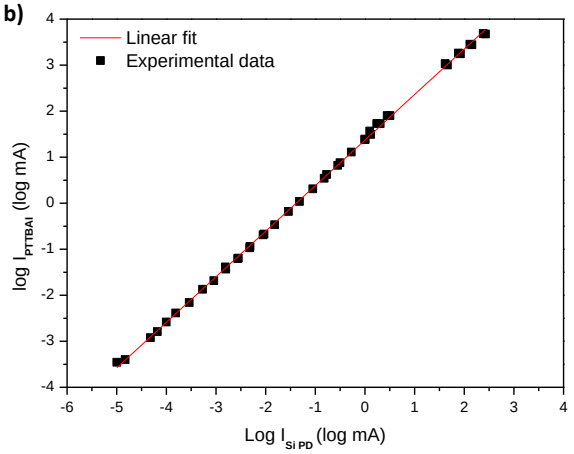

Figure 5. *a) Rise and fall time measurement for the **PTTBAI** device, showing the speed of the response to a light pulse with a frequency of 3000 Hz. b) Linear dynamic range for the NIR-OPD based on **PTTBAI** (with a silicon photodetector as reference), showing linearity over 7 orders of magnitude.*

Conclusions

Six different BAI-based push-pull type copolymers were synthesized, targeting maximum absorbance in the 900−1000 nm range. For **PTTBAI** and **PDFBBAI**, solubility issues hampered photodetector fabrication. Near-infrared organic photodetectors were constructed from the other four polymers – **PCPDTBAI**, **PTBAI**, **PTTBAI** and **PDTPBAI** – and their performances were investigated. The device based on **PTTBAI** demonstrated the best J_{ph}/J_D ratio, with a corresponding (shot-noise limited) detectivity of ~10^{12} Jones in the 600−1100 nm range. For **PCPDTBAI** and **PDTPBAI**, blend demixing was observed by AFM analysis, explaining the modest performances. Finally, the **PTTBAI** photodetector afforded a linear dynamic range of 145 dB, which is among the highest values reported so far, and a rise and fall time of 25 and 30 µs, respectively. As the targeted 940 nm region was successfully exploited, current efforts are directed towards the development of a prototype imager. Future work will aim to shift the absorption further into the NIR towards the so-called eye-safe region (1400−1500 nm), allowing the use of more powerful IR sources without hazard to the human eye.

Acknowledgements

F.V., S.G. and J.R. acknowledge the Research Foundation – Flanders (FWO Vlaanderen) for granting them a PhD fellowship. P.V. and J.K. are postdoctoral fellows of the FWO Vlaanderen. K.V. and W.M. are grateful for project funding by the FWO (G0D0118N and G0B2718N). Hasselt University and IMEC are partners in the SBO project MIRIS (Monolithic Infrared Image Sensors), supported by VLAIO (Vlaams Agentschap Innoveren en Ondernemen). The authors want to thank Geert Pirotte for his contribution to the MIRIS project.

References

1 H. Sirringhaus, *Adv. Mater.*, 2014, **26**, 1319–1335.
2 K. A. Mazzio and C. K. Luscombe, *Chem. Soc. Rev.*, 2015, **44**, 78–90.
3 X. Liu, Y. Lin, Y. Liao, J. Wu and Y. Zheng, *J. Mater. Chem. C*, 2018, **6**, 3499–3513.
4 X. Gong, M. Tong, Y. Xia, W. Cai, J. S. Moon, Y. Cao, G. Yu, C.-L. Shieh, B. Nilsson and A. J. Heeger, *Science*, 2009, **325**, 1665–1667.
5 J. Miao, F. Zhang, Y. Lin, W. Wang, M. Gao, L. Li, J. Zhang and X. Zhan, *Adv. Opt. Mater.*, 2016, **4**, 1711–1717.
6 M. Kielar, O. Dhez, G. Pecastaings, A. Curutchet and L. Hirsch, *Sci. Rep.*, 2016, **6**, 39201.

7 J. Qi, W. Qiao and Z. Y. Wang, *Chem. Rec.*, 2016, **16**, 1531–1548.
8 A. Rogalski, *Infrared Phys. Technol.*, 2002, **43**, 187–210.
9 P. K. Jain, X. Huang, I. H. El-Sayed and M. A. El-Sayed, *Acc. Chem. Res.*, 2008, **41**, 1578–1586.
10 X. Yi, F. Wang, W. Qin, X. Yang and J. Yuan, *Int. J. Nanomedicine*, 2014, **9**, 1347–1365.
11 A. Rogalski, *Prog. Quantum Electron.*, 2012, **36**, 342–473.
12 P. E. Malinowski, J.-Y. Duboz, P. De Moor, J. John, K. Minoglou, P. Srivastava, F. Semond, E. Frayssinet, B. Giordanengo, A. BenMoussa, U. Kroth, A. Gottwald, C. Laubis, R. Mertens and C. Van Hoof, *IEEE Electron Device Lett.*, 2011, **32**, 1561–1563.
13 X. Chen, X. Lu, B. Deng, O. Sinai, Y. Shao, C. Li, S. Yuan, V. Tran, K. Watanabe, T. Taniguchi, D. Naveh, L. Yang and F. Xia, *Nat. Commun.*, 2017, **8**, 1672.
14 R. W. Hoogeveen, R. J. van der A and A. P. Goede, *Infrared Phys. Technol.*, 2001, **42**, 1–16.
15 A. Rogalski, *Prog. Quantum Electron.*, 2003, **27**, 59–210.
16 J. B. D. Soole and H. Schumacher, *IEEE J. Quantum Electron.*, 1991, **27**, 737–752.
17 K.-J. Baeg, M. Binda, D. Natali, M. Caironi and Y.-Y. Noh, *Adv. Mater.*, 2013, **25**, 4267–4295.
18 L. Dou, Y. Liu, Z. Hong, G. Li and Y. Yang, *Chem. Rev.*, 2015, **115**, 12633–12665.
19 A. E. London, L. Huang, B. A. Zhang, M. B. Oviedo, J. Tropp, W. Yao, Z. Wu, B. M. Wong, T. N. Ng and J. D. Azoulay, *Polym. Chem.*, 2017, **8**, 2922–2930.
20 J. Han, J. Qi, X. Zheng, Y. Wang, L. Hu, C. Guo, Y. Wang, Y. Li, D. Ma, W. Qiao and Z. Y. Wang, *J. Mater. Chem. C*, 2017, **5**, 159–165.
21 H. Zhou, L. Yang, S. Stoneking and W. You, *ACS Appl. Mater. Interfaces*, 2010, **2**, 1377–1383.
22 L. Zheng, T. Zhu, W. Xu, L. Liu, J. Zheng, X. Gong and F. Wudl, *J. Mater. Chem. C*, 2018, **6**, 3634–3641.
23 J. Brebels, K. C. C. W. S. Klider, M. Kelchtermans, P. Verstappen, M. Van Landeghem, S. Van Doorslaer, E. Goovaerts, J. R. Garcia, J. Manca, L. Lutsen, D. Vanderzande and W. Maes, *Org. Electron.*, 2017, **50**, 264–272.
24 B. He, A. B. Pun, D. Zherebetskyy, Y. Liu, F. Liu, L. M. Klivansky, A. M. McGough, B. A. Zhang, K. Lo, T. P. Russell, L. Wang and Y. Liu, *J. Am. Chem. Soc.*, 2014, **136**, 15093–15101.
25 B. He, D. Zherebetskyy, H. Wang, M. A. Kolaczkowski, L. M. Klivansky, T. Tan, L. Wang and Y. Liu, *Chem. Sci.*, 2016, **7**, 3857–3861.
26 B. He, W. T. Neo, T. L. Chen, L. M. Klivansky, H. Wang, T. Tan, S. J. Teat, J. Xu and Y. Liu, *ACS Sustain. Chem. Eng.*, 2016, **4**, 2797–2805.
27 K. J. Fallon, N. Wijeyasinghe, N. Yaacobi-Gross, R. S. Ashraf, D. M. E. Freeman, R. G. Palgrave, M. Al-Hashimi, T. J. Marks, I. McCulloch, T. D. Anthopoulos and H. Bronstein, *Macromolecules*, 2015, **48**, 5148–5154.
28 J. Zhu, T. Li, K. Shi, J. Wang, Y. Lin, G. Yu and X. Zhan, *J. Polym. Sci. Part A Polym. Chem.*, 2017, **56**, 213–220.
29 *Ullmann's Encyclopedia of Industrial Chemistry*, Wiley-VCH Verlag GmbH & Co. KGaA, Weinheim, Germany, 2000.
30 Technical note: optical detection systems, Newport catalogue, https://www.newport.com/n/optical-detection-systems, (accessed June 2018)
31 M. A. Kolaczkowski, B. He and Y. Liu, *Org. Lett.*, 2016, **18**, 5224–5227.
32 D.-J. Cai, P.-H. Lin and C.-Y. Liu, *Eur. J. Org. Chem.*, 2015, 5448–5452.
33 H. Zhou, L. Yang and W. You, *Macromolecules*, 2012, **45**, 607–632.
34 A. Rudnick, C. Wetzel, S. Tscheuschner, H. Schmalz, A. Vogt, A. Greiner, H. Bässler, E. Mena-Osteritz, P. Bäuerle and A. Köhler, *J. Phys. Chem. B*, 2017, **121**, 7492–7501.
35 S. H. Eom, S. Y. Nam, H. J. Do, J. Lee, S. Jeon, T. J. Shin, I. H. Jung, S. C. Yoon and C. Lee, *Polym. Chem.*, 2017, **8**, 3612–3621.
36 L. Zhang, T. Yang, L. Shen, Y. Fang, L. Dang, N. Zhou, X. Guo, Z. Hong, Y. Yang, H. Wu, J. Huang and Y. Liang, *Adv. Mater.*, 2015, **27**, 6496–6503.
37 A. Armin, M. Hambsch, I. K. Kim, P. L. Burn, P. Meredith and E. B. Namdas, *Laser Photonics Rev.*, 2014, **8**, 924–932.
38 Q. Lin, A. Armin, D. M. Lyons, P. L. Burn and P. Meredith, *Adv. Mater.*, 2015, **27**, 2060–2064.